Geoscience Letters

RESEARCH LETTER

Open Access

Identifying the shift in global wildfire weather conditions over the past four decades: an analysis based on change-points and long-term trends

Ke Shi[1*] and Yoshiya Touge[2]

Abstract

Most of studies on change-point at a regional or global scale have only examined a single hydrometeorological variable and have been unable to identify any underlying explanations. In this study, we identified change-points and long-term trends of six wildfire-related variables and attempted to explain the cause of change-point from atmospheric–oceanic indices. As a result, we discovered that the main change-point dates for the precipitation, temperature, and drought codes, as well as the duff moisture code, fine fuel moisture code, and fire weather index, were 1995–2000 and 2000–2005, respectively. Furthermore, the relationship between the change-point of six variables and atmospheric–oceanic indices was discussed through the correlation coefficient. For example, the Atlantic Multidecadal Oscillation was found to dominate the precipitation in West Africa. In addition, we divided the globe into eight homogenous wildfire weather zones based on the change-point dates and long-term trends of the six variables.

Keywords Change-point, Wildfire weather, Trend, Global

Introduction

The nonstationarity in hydrometeorological variables, such as precipitation (Dhakal et al. 2015; Gu et al. 2019; Vu and Mishra, 2019), temperature (Aziz et al. 2020; Carney et al. 2020; Kärner, 2002), and drought index (Das et al. 2020; Kwon and Lall, 2016; Wu et al. 2020), has been extensively studied. Most of the existing research has focused on the long-term trends of hydrometeorological variables (Byakatonda et al. 2018; Meshram et al. 2017; Salman et al. 2017) and on the change-points in these variables (Ahmadi et al. 2018; Jiang et al. 2019; Liu et al. 2020). Such studies have discovered that, under the increasing influence of global warming, more high temperature events and extreme droughts have shown increasing trends of occurrence in the United States (Ge et al. 2016), China (Ye et al. 2019), Southeast Asia (Dong et al. 2021), Australia (Sharples et al. 2021), and Brazil (Geirinhas et al. 2021). And one of the prominent consequences is increased wildfire risk (Mukherjee et al. 2018).

The change-points of hydrometeorological variables have been widely investigated at the regional scale (e.g., Deng et al. 2018; Ouhamdouch and Bahir, 2017)), but only a few studies have examined the connections among the change-points of different variables at the global scale. Unlike the long-term trend of the external forcing caused by anthropogenic climate change, the change-points are often assumed to be an indicator of natural climate variability (Ivancic and Shaw 2017). An abrupt change in a hydrometeorological variable has impacts on other variables, resulting in a multifaceted effect.

*Correspondence:
Ke Shi
ke.dlut@outlook.com
[1] Department of Civil and Environmental Engineering, Tohoku University, Sendai, Miyagi 980-8579, Japan
[2] Disaster Prevention Research Institute, Kyoto University, Uji, Kyoto 611-0011, Japan

For example, increasing temperature and decreasing precipitation were the main drivers responsible for the change-point of drought frequency in Inner Mongolia in the 2000s (Liu et al. 2016). In addition, in the mid-1980s, an abrupt increase in large wildfires was observed in the forests of the western United States in early spring under the influence of global warming (Westerling et al. 2006). Such rapid increases in the occurrence of wildfires during the twenty-first century have also been observed in the Pacific Northwest forests of the United States driven by earlier spring snowmelt, warmer temperatures, and reduced winter precipitation (O'Dell et al. 2019). Nevertheless, the cumulative effect of shifts in global wildfire weather conditions and the causes of these shifts remain uncertain.

Compared with traditional hydrometeorological variables, wildfire variables (e.g., burned area and number of wildfires) are influenced by multiple factors, such as the fuel characteristics and weather conditions (Trollope et al. 2002). Unfortunately, previous studies did not explore this thoroughly. Therefore, since certain weather conditions are essential prerequisites for wildfires (Qu et al. 2021), it is urgently necessary to improve our understanding of the abrupt changes and long-term trend of wildfire weather. Overall, the existing studies (Liu et al. 2016; O'Dell et al. 2019; Westerling et al. 2006) have only sparingly accounted for the impact of abrupt changes in weather conditions on wildfires from a global perspective, and the mechanisms responsible for these abrupt changes have yet to be fully elucidated.

Accordingly, this paper attempts to identify the change-points and long-term trends of multiple weather variables related to wildfires based on the Pettitt test (Pettitt 1979) and trend-free prewhitening Mann–Kendall (TFPW-MK) test (Yue and Wang 2002), respectively. Then, the causes of abrupt change are discussed through correlation analysis between atmospheric–oceanic indices and wildfire-related variables. Finally, by applying the clustering method outlined by Scrucca (Scrucca et al. 2016), grids with similar change-points in time and similar wildfire weather change trends are clustered. Consequently, maps of global wildfire weather changes are constructed, which are expected to provide a new perspective on wildfire weather conditions over the past four decades.

Materials and methods

In this paper, we selected six wildfire-related meteorological variables: daily precipitation, daily maximum temperature (Tmax), drought code, fine fuel moisture code, duff moisture code, and fire weather index. In addition, four commonly used atmospheric–oceanic indices were selected to analyze the possible causes of change-points, including the Pacific Decadal Oscillation Index (PDO), Multivariate El Niño–Southern Oscillation Index (MEI), Atlantic Multi-decadal Oscillation Index (AMO), and Dipole Mode Index (DMI). All global atmospheric–oceanic indices are on a monthly scale and come from the National Oceanic and Atmospheric Administration. Daily precipitation and Tmax data during 1979–2020 with a spatial resolution of 0.5° were obtained from the Climate Prediction Center (CPC) Global Unified Gauge-Based Analysis of Daily Precipitation (Chen et al. 2008; Xie et al. 2010, 2007) and the CPC global daily surface 2-m air temperature analysis (Pan et al. 2019), respectively. Drought code, fine fuel moisture code, duff moisture code, and fire weather index data during 1979–2020 with a spatial resolution of 0.5° were extracted from fire danger indices historical data from the Copernicus Emergency Management Service. Global wildfire data is from the Fire CCI v5.1 data set during 2001–2020 developed by Chuvieco et al. (2018), which is based on a hybrid approach combining the highest resolution (250 m) near-infrared band of MODIS with active wildfire information. In addition, the wildfire data were processed to a 0.5° spatial resolution consistent with wildfire-related variables. Then, we removed grids that never had a wildfire event (e.g., the Sahara desert). Of the 32,599 grids retained, those grids that did not contain at least one value per month were removed, for a total of 48 grids. As final, the total number of grids used for the calculation is 32,551. Then, for each remaining grid, we aggregated the daily values into time series of maximum monthly values to show the extreme dry/wet conditions each month. To reduce the possible impact of missing records, we extracted the maximum daily value of each month and processed the six wildfire-related variables into monthly time series. In addition, the climate reference zones (IPCC 2014) were applied to indicate different regions, as shown in Fig. 1.

For wildfire-related variables excluding precipitation and temperature, fine fuel moisture code, duff moisture code, and drought code represent moisture conditions of fine dead surface fuels, loosely compacted organic material on the forest floor, and deep organic soil layer, respectively. All three of them are unitless and larger values indicate lower fuel moisture conditions. In particular, under cover of a forest canopy, fuel moisture of forest litter fuels is represented by the fine fuel moisture code (range from 0 to 101). This index is calculated based on daily precipitation, relative air humidity, wind speed, and air temperature data. It represents moisture conditions for shaded litter fuels, the equivalent of a 16-h time-lag. The duff moisture code is calculated using daily precipitation, relative air humidity, and air temperature data taken at mid-day, indicating slow-drying surface fuels (12-day time-lag). The drought code, a unitless index, is calculated from daily precipitation and air temperature,

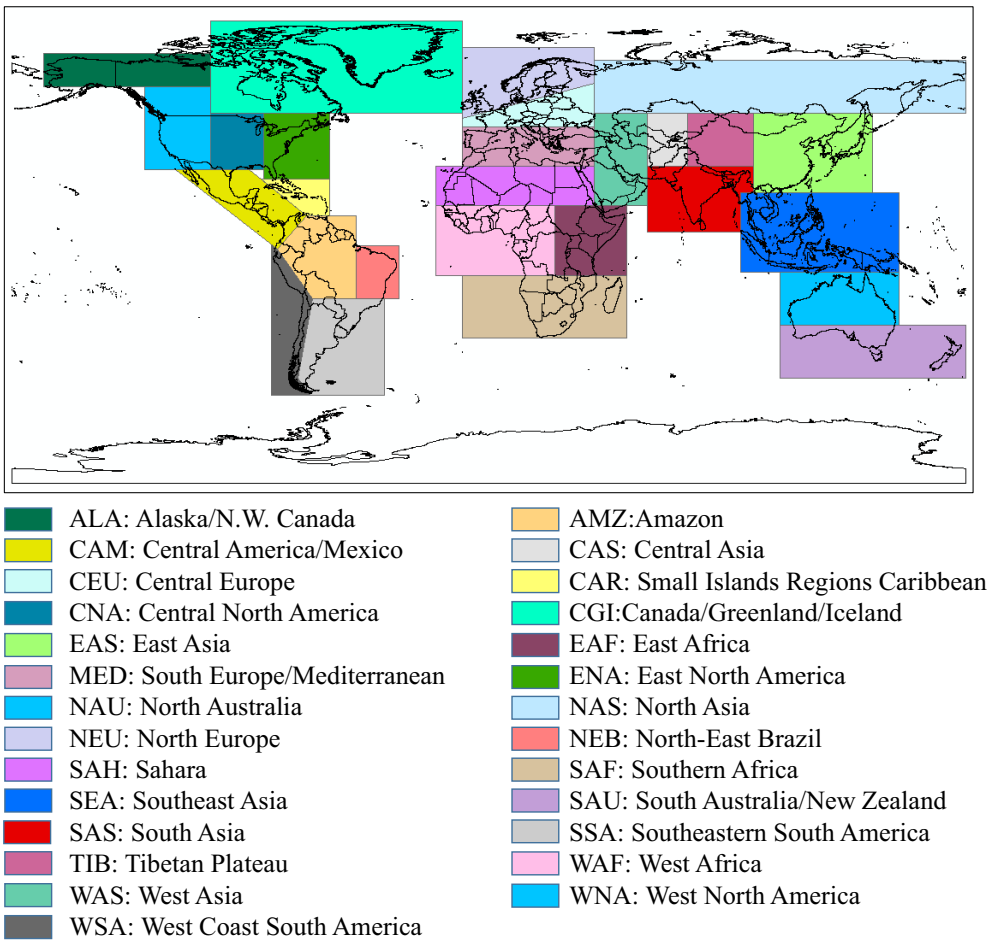

Fig. 1 Spatial boundaries of the geographical regions based on the IPCC 5th Assessment Report. This map shows the locations and boundaries of 27 climate reference regions

representing the fuels with an extremely sluggish drying rate (53-day time-lag). The maximum value of the drought code is 1000, and values over 800 indicate extreme drought conditions. The fire weather index is a comprehensive fire behavior index that considers the fire spread potential and potential energy release under the premise of considering fuel conditions. It is a unitless dimensionless index rating the potential fire line intensity given the meteorological conditions for a reference fuel type. Although the fire weather index was developed for the boreal forests of Canada, it has proven to be a useful indicator in Portugal (Carvalho et al. 2008), China (Tian et al. 2011), France (Fox et al. 2018), and many parts of the world (Bedia et al. 2015).

The Pearson correlation coefficient was used to detect the correlation between the two variables. The Pearson method assesses the correlation coefficient of two conditioning factors. The correlation value is calculated by their covariance divided by the product of their standard deviations. Pearson correlations are represented in square tables called correlation matrices, which compute Pearson correlations for each column pair of a set of variables. Each matrix value represents the calculated correlation of the corresponding row and column variables (Tehrany et al. 2019). The data used for the correlation analysis were all on a monthly scale. Although different climate oscillation have different interannual or multi-decades variations, stronger correlations will be detected when the pattern of this variation is similar to the periodicity of wildfire-related variables.

To evaluate abrupt changes, a nonparametric Pettitt test was utilized to detect change-points (Pettitt, 1979). The Pettitt test is one of the most widely applied tests to determine abrupt shifts in hydrometeorological time series around the world (Addisu et al. 2015; Asfaw et al. 2018; Ayamga et al. 2021; Ca 2017). Compared with other similar approaches, such as binary segmentation (Scott and Knott, 1974), Bayesian analysis (Erdman

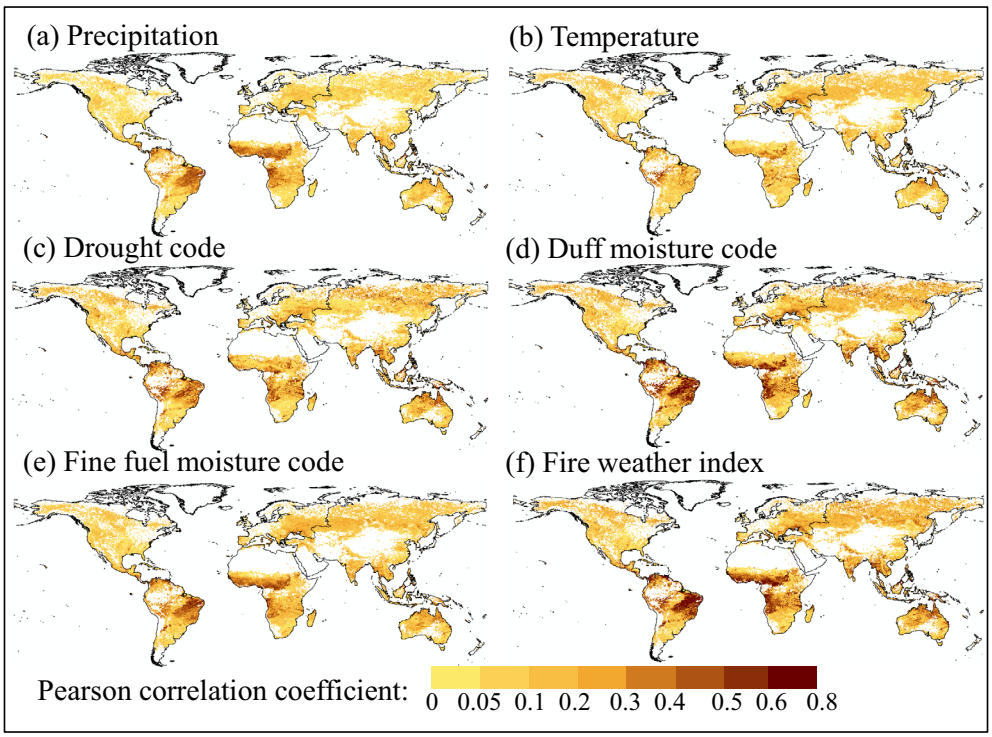

Fig. 2 Pearson correlation coefficient plot of wildfire-related variables and burned area. The blank area in this figure is the area without any wildfire data. This figure shows the spatial distribution of correlation coefficients between six wildfire-relatedvariables and burned area from 2001 to 2020

and Emerson 2008), wild binary segmentation (Fryzlewicz, 2014) and the nonparametric pruned exact linear time method (Haynes et al. 2017), the Pettitt test was found to deliver the best change-point detection results while simultaneously minimizing the number of false positives (Slater et al. 2021). After passing a significance test, the change-point date and change trend of each of the six wildfire-related meteorological variables in each grid were recorded. Beaulieu et al. (2012) used artificial time series to test the sensitivity of sequence time length on change-point testing. They found that the false alarms will be higher when the change-point appears near the beginning and end of the time series. In addition, the time series of at least 4 years can detect possible change-points. That is, mutation points detected over a 4-year-long period at the beginning and end were more prone to false alarms (Beaulieu et al. 2012). In this study, change-point dates were counted every 5 years, and this study set the time period for removal as 5 years (longer than the minimum 4-year threshold) to facilitate the presentation of statistical results. Thus, in this study, we removed the change-points detected during 1979–1983 and 2016–2020. In addition, all data were pre-whitened and detrended prior to change-point testing to avoid the influence of time series autocorrelation and long-term trend.

Next, to show the trends of the global changes in these variables more clearly, we extracted the grids that passed the significance test of the change-points and divided them into time series averaged over 27 climate reference regions for four seasons. Similarly, the data (time series of the four seasons) used for trend detection was also pre-whitened and detrended before the Mann–Kendall trend test, which is called trend-free prewhitening Mann–Kendall (TFPW-MK) test(Yue and Wang 2002). It is an improved version of the MK test proposed by Mann (Mann, 1945) and modified by Kendall (Kendall, 1948) that is widely used to analyze the change trends of hydrometeorological time series (Liu et al. 2015). The MK test requires that the data be independent. However, some hydrometeorological time series often display a serial correlation, which increases the probability that the MK test can detect a significant trend, thereby altering the estimated magnitude of the serial correlation (Yue and Wang 2002). And the TFPW-MK test can efficiently eliminate the effect of such serial correlations on the MK trend test.

Finally, the change-point date and trend of each of these six variables were adopted as input data for clustering. The Mclust toolkit (Scrucca et al. 2016) based on R was used to perform a cluster analysis on the comprehensive data set. This process comprises three elements:

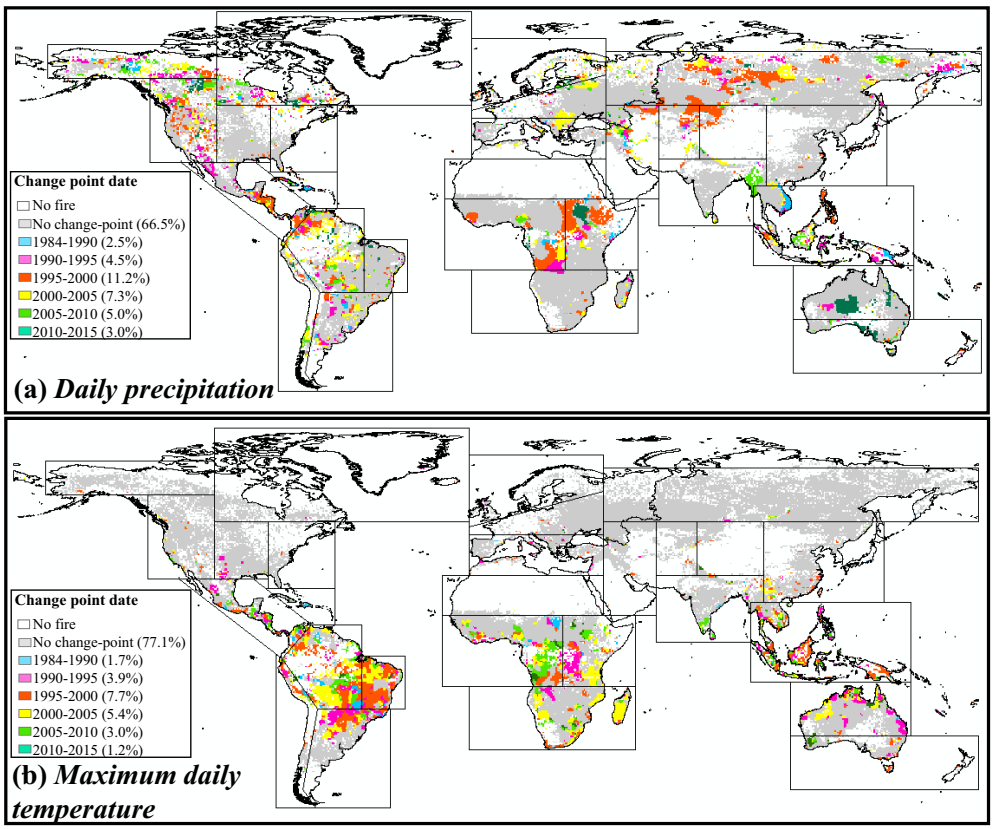

Fig. 3 Global map-1 showing the distributions of the change-points. This global map-1 shows the distributions of the change-points of the daily precipitation andmaximum daily temperature on a monthly scale. The map is marked with grids of significantchange-points, where different colors indicate when an abrupt change occurs. Blanks in the figureindicate areas without wildfires. Numbers in parentheses indicate the percentage of change-pointdates

(1) initialization via model-based hierarchical agglomerative clustering; (2) maximum likelihood estimation via the expectation–maximization (EM) algorithm (Bradley et al. 1998; Dempster et al. 1977); and (3) selection of the Bayesian model and the number of clusters using approximate Bayes factors with a Bayesian information criterion approximation (Fraley and Raftery 2002; Fraley et al. 2012; Scrucca et al. 2016). Unlike traditional clustering methods, such as k-means clustering (MacQueen 1967) and Ward's method (Ward Jr 1963), the Mclust toolkit can solve three key problems: how many clusters there should be, which clustering method should be used, and how outliers should be handled.

Results and discussions

Before the change-points and long-term trends analysis of six wildfire-related variables, we first calculated the Pearson correlation coefficients between six wildfire-related variables and the burned area from 2001 to 2020, as shown in Fig. 2. Among the six wildfire-related variables, there was the strongest correlation between the fire weather index and burned area, especially in South America and Africa. A similar distribution of correlation coefficients was also found for the duff moisture code, but the areas with high (Fig. 2) correlation coefficients in Africa were less than the fire weather index. The correlation coefficients of precipitation, drought code, and fine fuel moisture code also have similar distributions but with relatively small correlation coefficient values. Conversely, there was a weak correlation between temperature and burned area, even in South America and Africa. These results suggest that additional attention should be paid to areas with a high correlation to burn area (such as parts of South America and Africa) in the subsequent analysis of change-points and trends. The six variables in the weakly correlated regions should be interpreted as potential wildfire-related variables rather than wildfire-related variables.

Based on the proposed change-point detection algorithm and circular statistical approach, the global change-point dates of the six wildfire-related variables are shown in Figs. 3, 4, and 5. The global change-point map conveys

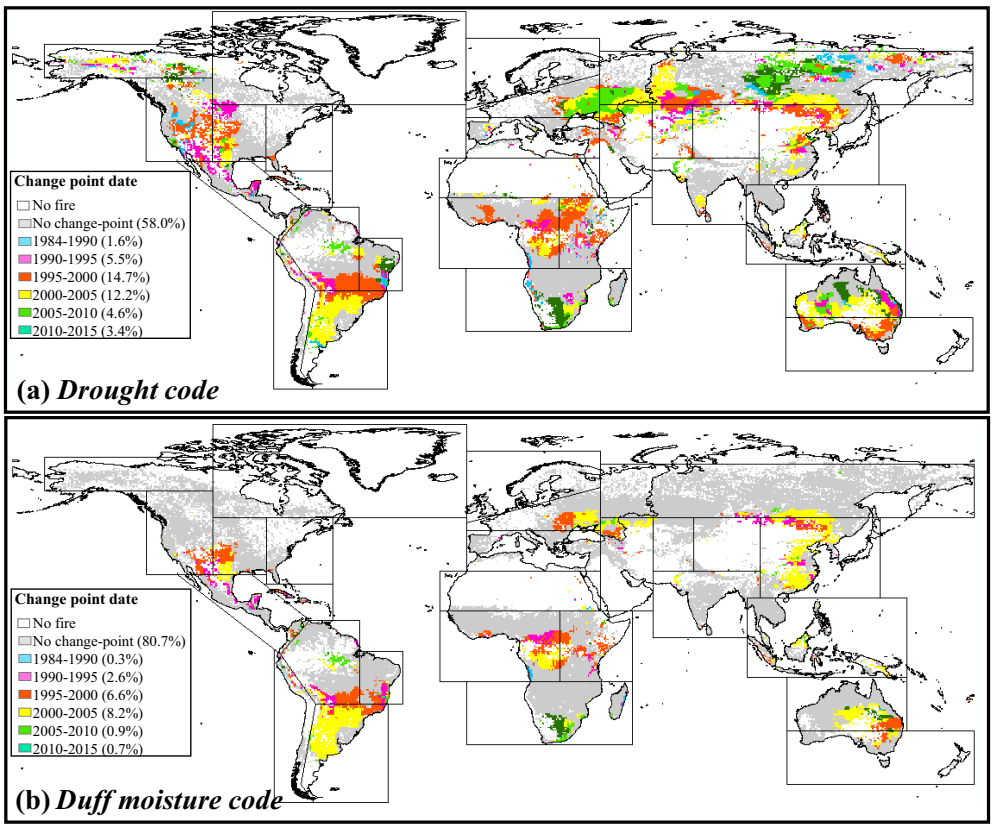

Fig. 4 Global map-2 showing the distributions of the change-points. This global map-2 shows the distributions of the change-points of the drought code and duffmoisture code on a monthly scale. The map is marked with grids of significant change-points,where different colors indicate when an abrupt change occurs. Blanks in the figure indicate areaswithout wildfires. Numbers in parentheses indicate the percentage of change-point dates

interesting information, as all six wildfire-related variables exhibit varying characteristics in different parts of the globe. In addition, Figs. 6 and 7 summarize the proportion of change-point dates and change trend for the six variables in the 27 reference regions, respectively, to more clearly present the interesting findings obtained in this paper.

For the daily precipitation (Figs. 3a, 6a, and 7a), 1995–2000 was the period with the highest number of change-points, accounting for 11.2% of the total grid. In addition, the major change-point dates varied by region, and change trends were predominantly increasing after the change-point in SEA, TIB, NEU, and ALA regions accounting for more than 30%. However, precipitation in CGI, CAR, AMZ, WSA, and EAF regions showed decreasing trend after the change-point. As for the change-point dates, the five regions, TIB, CAM, CAR, EAF, and CAS, were mainly concentrated in 1995–2000. In particular, the change-point dates in the TIB region were almost all from 1995 to 2000. On the other hand, the change-point dates in the AMZ and WSA regions of South America were mainly from 2000 to 2005. SAU and NAU were two regions with sudden changes in precipitation during 2010–2015.

For the maximum daily temperature (Figs. 3b, 6b, and 7b), the main change-point dates for temperature were 1995–2000, followed by 2000–2005. The abrupt changes in temperature in the southern hemisphere were more pronounced than those in the northern hemisphere, especially the NEB, WSA, and AMZ in South America. The change-point dates in the NEB and WSA regions were mainly concentrated in 1995–2000, while 1995–2005 was the period of temperature mutation in AMZ. Except for the WSA, the temperature in other places mainly showed an increasing trend after the change-point. Comparing Fig. 3a with Fig. 3b reveals that the precipitation and temperature both show decreasing change trends in the WSA region.

From Figs. 4a, 6c, and 7c, the drought code was detected with the highest number of change-points in the six wildfire-related variables, with 14.7% and 12.2% of change-point dates in the periods 1995–2000

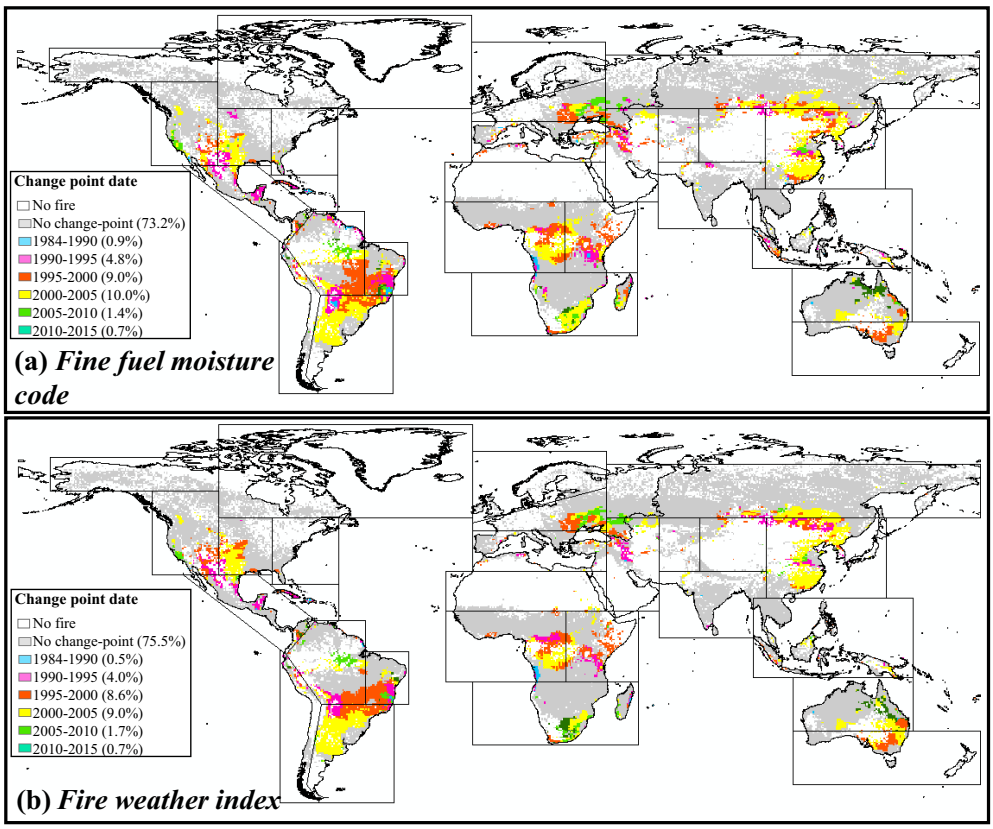

Fig. 5 Global map-3 showing the distributions of the change-points. This global map-3 shows the distributions of the change-points of the fine fuel moisture and fireweather index on a monthly scale. The map is marked with grids of significant change-points,where different colors indicate when an abrupt change occurs. Blanks in the figure indicate areaswithout wildfires. Numbers in parentheses indicate the percentage of change-point dates

and 2000–2005, respectively. The abrupt changes in the drought code of SAU, CAR, and EAF were mainly concentrated in 1995–2000. SSA, NAU, EAS, and WAS were the four regions with the most percentage of change-point dates from 2000 to 2005. In addition, the NAS, CEU, and WAS regions also showed abrupt changes in the drought code between 2005 and 2010. The change-point distribution patterns of the duff moisture code, fine fuel moisture code, and fire weather index are similar (Figs. 4b, 5, 6d–f, and 7d–f). Change-points in these three variables occurred most frequently during the period 2000–2005. The duff moisture code was detected with the fewest change-points in these six variables. The change-point dates for these three variables in the SSA and EAS regions were mainly concentrated in 2000–2005. Excluding the duff moisture code, 2000–2005 and 1995–2000 were periods of change-point of the other two variables in the CNA and SAU regions, respectively. In addition, the change-point date of the duff moisture code was 1995–2005 in the CNA region. The CAR and CAM of these three variables were the regions, where the change-points occurred in 1990–1995.

Furthermore, the change zone surrounding the coast of the Peru–Chile Trench (WSA region) was the region affected by El Niño and La Niña among other climate variability phenomena (Takahashi 2004). Strong El Niño events swept this region during 1997–1998, followed by strong La Niña events during 1998–2000. The strong El Niño of 1997–1998 brought heavy precipitation to the coast of the Peru–Chile Trench but did not bring significant rainfall to the central Chilean Atacama (Kane 1999; McKay et al. 2003; Sanabria et al. 2018). After the significant increase in precipitation in 1997–1998, strong La Niña led to a sharp decrease in precipitation (Glantz 2001; Larrain et al. 2001). In addition, this change-point in precipitation was detected in our study between 2000 and 2005. Moreover, as seen from Fig. 8a–d, MEI and PDO have higher correlation coefficients than most regions of the world for the WSA southern region. These findings could verify the impact of ENSO on the sudden change in precipitation in the region, and this study

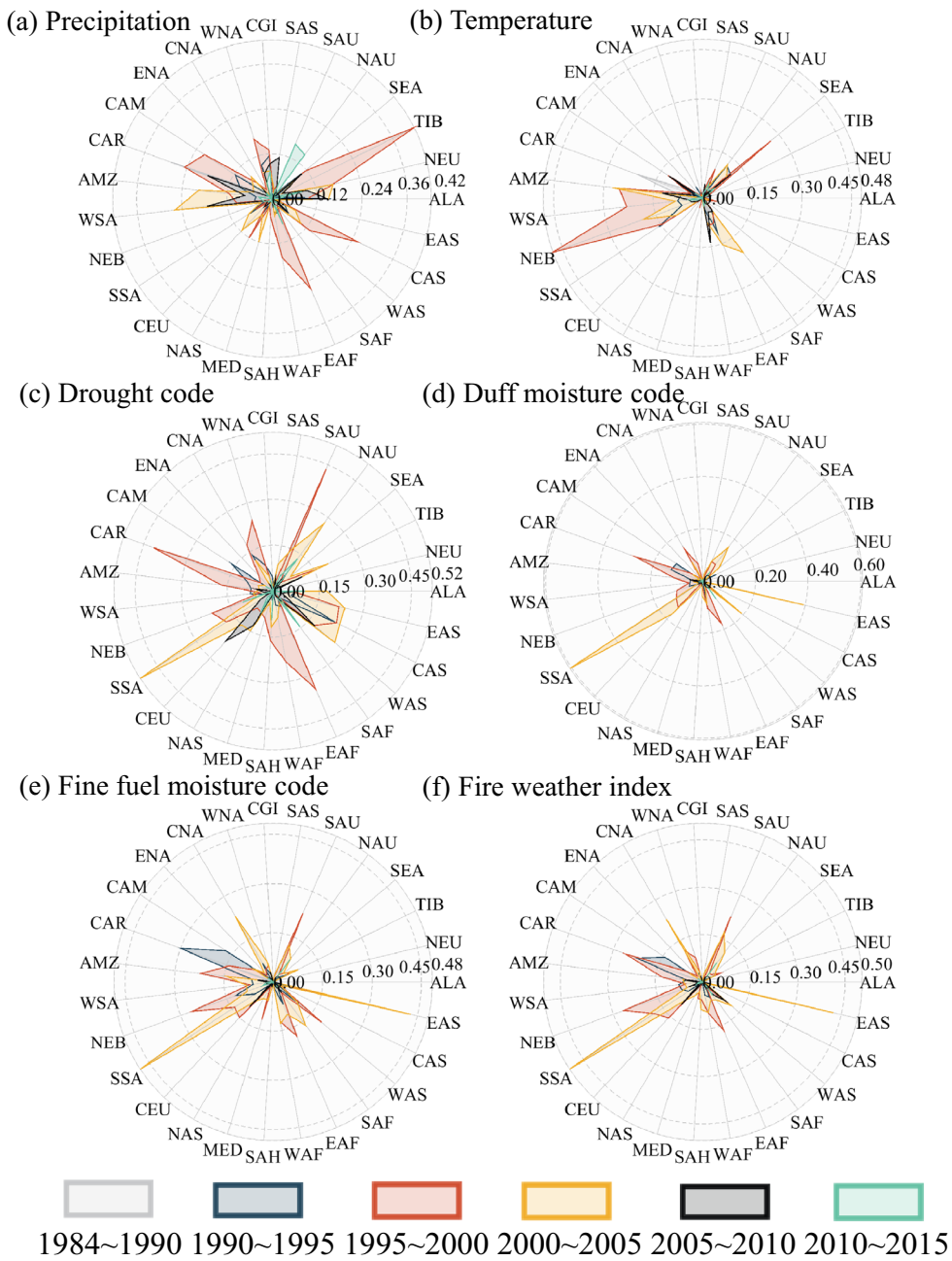

Fig. 6 Percentage of change-point dates in 27 climate reference regions. This figure shows the proportion of each change-point date in the 27 climate reference regions

also found that PDO also contributed to this precipitation variation. In addition, among the four atmospheric–oceanic indices, AMO had a strongest impact on the WAF region, corresponding to the abrupt changes that occurred in this region during 2000–2005.

Global warming increases water vapor in the atmosphere, resulting in enhanced precipitation over wet (ascending) regions and reduced precipitation over dry (descending) regions (Chou et al. 2013). In addition, the dependence of extreme precipitation and temperature is more significant over short durations in coastal regions (Panthou et al. 2014). Accordingly, our change trend results provide evidence that the precipitation and temperature variation characteristics along the coast of the Peru–Chile Trench are the same. The change-points of Africa varied significantly among different regions and

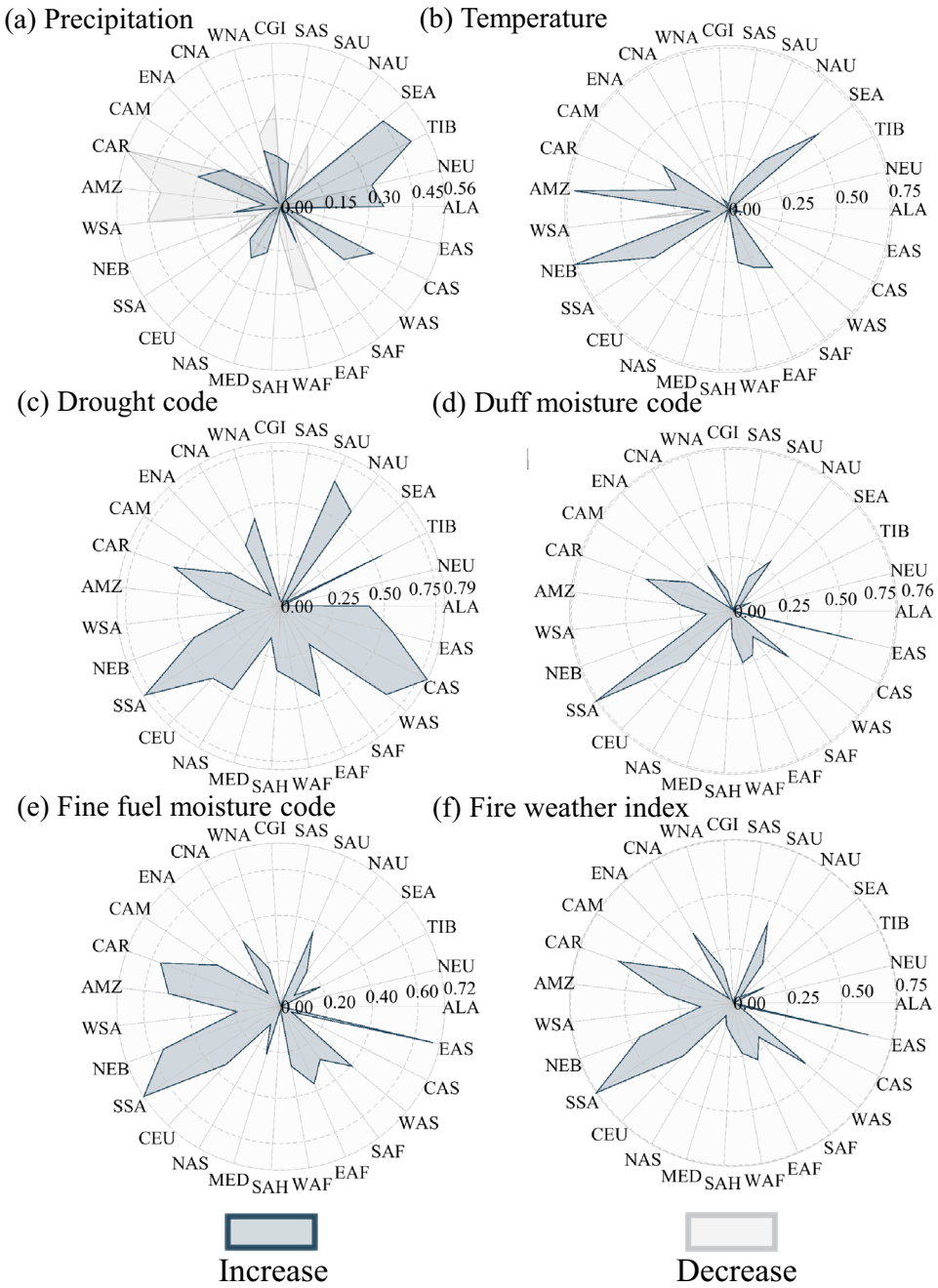

Fig. 7 Percentage of change trend in 27 climate reference regions. The figure shows the proportion of each change trend in the 27 climate reference regions

were concentrated mainly in the four time periods of 1990–1995, 1995–2000, 2000–2005, and 2005–2010. In addition, there were many increasing change-points in the SEA region during 1995–2000. In contrast to its impact on coastlines in the eastern Pacific, the strong El Niño during 1997–1998 brought less precipitation and high temperature to the SEA region (Tangang et al. 2017). Under the influence of global warming, this strong El Niño has further aggravated the rate of temperature rise in the SEA region. As a result, the period of 1997–1998 was a significant change-point date of temperature variability in the SEA region. From Fig. 8e–h, all four climatic drivers had an impact on the SEA region, but the location of the impact varied. Among them, PDO and MEI mainly affect temperature in the eastern part of the SEA, while AMO and DMI mainly affect temperature in the

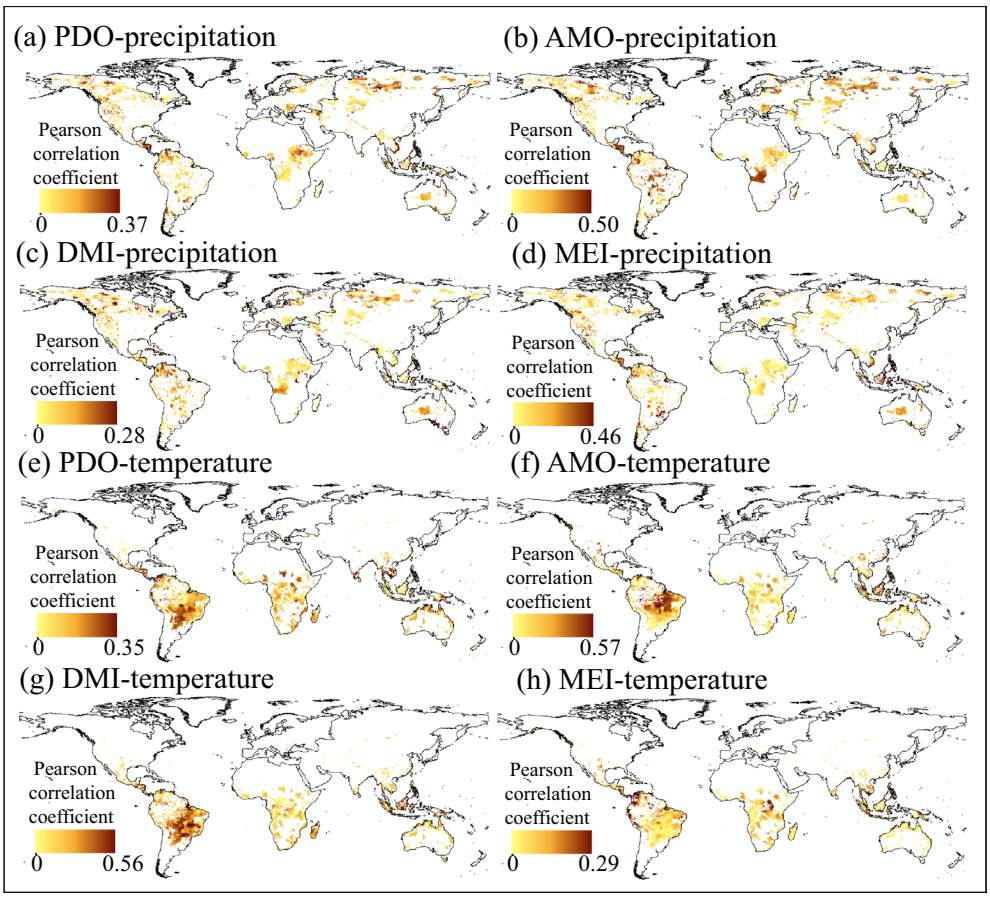

Fig. 8 Distribution map-1 of correlation coefficients of atmospheric–oceanic indices and wildfire-related variables. This dstribution map-1 shows the effects of the four atmospheric-oceanic indices on precipitationand temperature through pearson correlation coefficients. Blank indicates that no wildfires orchange-points have occurred on the grid. PDO: Pacific Decadal Oscillation Index. MEI:Multivariate El Niño-Southern Oscillation Index. AMO: Atlantic Multi-decadal Oscillation Index.DMI: Dipole Mode Index

western part of the SEA. Moreover, the effects of AMO and DMI on the AMZ and NEB regions were also worthy of attention, and a large number of change-points have been detected in these two regions.

Several studies have found a significant shift toward a greater annual burned area and a greater percentage of highly severe fires burning in the CNA region in 2000 (Abatzoglou and Williams 2016; Mueller et al. 2020). In comparison, our results show that the abrupt changes in fuel moisture and wildfire weather actually occurred earlier than the 2000 shift in the burned area. That is, the characteristics of fuel moisture and wildfire weather had undergone abrupt changes before 2000, which provided drier fuel and more fire-prone weather conditions for the subsequent shift in the burned area. In addition, from Figs. 9 and 10, the MEI had significant effects on the duff moisture code, fine fuel moisture code, and fire weather index in the CNA region, which suggested that El Niño–Southern Oscillation had some control over fire weather conditions in the region. For SSA region, the change-point distribution of the duff moisture code, fine fuel moisture code, and fire weather index is consistent with that of the drought code. Moreover, the increasing drought trend in this region was also reported by Damberg et al. (Damberg and AghaKouchak 2014). Ultimately, drier weather was the dominant factor affecting fuel and fire weather changes. In addition, since the early 2000s, higher-than-average fire weather has been more frequent in the SAU region, especially during the most severe season of 2002–2003 (Harris and Lucas 2019). According to our results, 2000–2005 was also a concentrated period of abrupt changes in drought, fuel, and fire weather. Figures 9 and 10 show that the PDO and MEI are the atmospheric–oceanic indices in both the SSA and SAU regions, respectively.

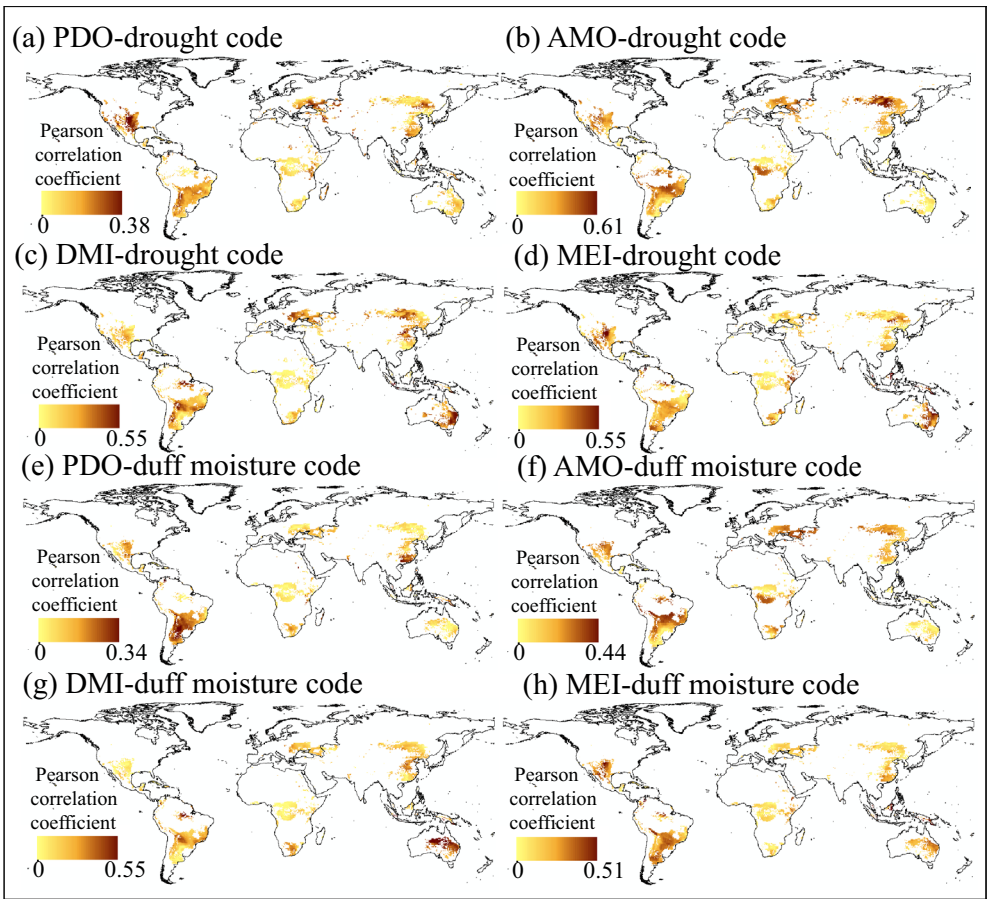

Fig. 9 Distribution map-2 of correlation coefficients of atmospheric–oceanic indices and wildfire-related variables. This dstribution map-2 shows the effects of the four atmospheric-oceanic indices on drought codeand duff moisture code through pearson correlation coefficients. Blank indicates that no wildfiresor change-points have occurred on the grid. PDO: Pacific Decadal Oscillation Index. MEI:Multivariate El Niño-Southern Oscillation Index. AMO: Atlantic Multi-decadal Oscillation Index.DMI: Dipole Mode Index

Regarding the seasonal trends, Fig. 11 shows the change trends of the six variables over 27 climate reference regions in different seasons (only for the grids, where a change-point was detected). As for precipitation, the trends are the same for most regions in all seasons (all increasing or decreasing). The SAU area showed an increase in precipitation only in spring, with decreasing trends in all other seasons. In addition, spring precipitation showed a decline in the CAM region and an increase in winter, remaining almost constant between the summer and autumn seasons. Similar regions of inconsistent seasonal variation were found in NEU, SAU, SAS, etc. Temperatures showed a significant decreasing trend in summer and autumn in the WSA region, while the trend in spring and winter was not significant. Other regions showed a significant increasing trend or no significant change in temperature. In addition, the NEB region was the most significant warming of the 27 climate reference regions. Of the other four variables, the most significant increasing trends were for drought code in winter and duff moisture code, fine fuel moisture code, and fire weather index in autumn. A similar strong increasing trend was observed for drought code in the NEB winter and three other variables in the CEU autumn.

To better understand such a large amount of information about the change-points of different variables, we performed clustering to integrate the information (Fig. 12). A stationarity zone refers to a region, where no change-point was detected in any variable, whereas intensified drought zones and weakened drought zones denote the regions dominated by a change-point in the drought code, although the change trends of these two zones have opposite signs (increasing and decreasing, respectively). The grids where only precipitation exhibits abrupt changes are concentrated in precipitation-dominated zones. In the drought–precipitation interaction zone, abrupt changes in drought and precipitation occur in the same region but in different periods. In addition,

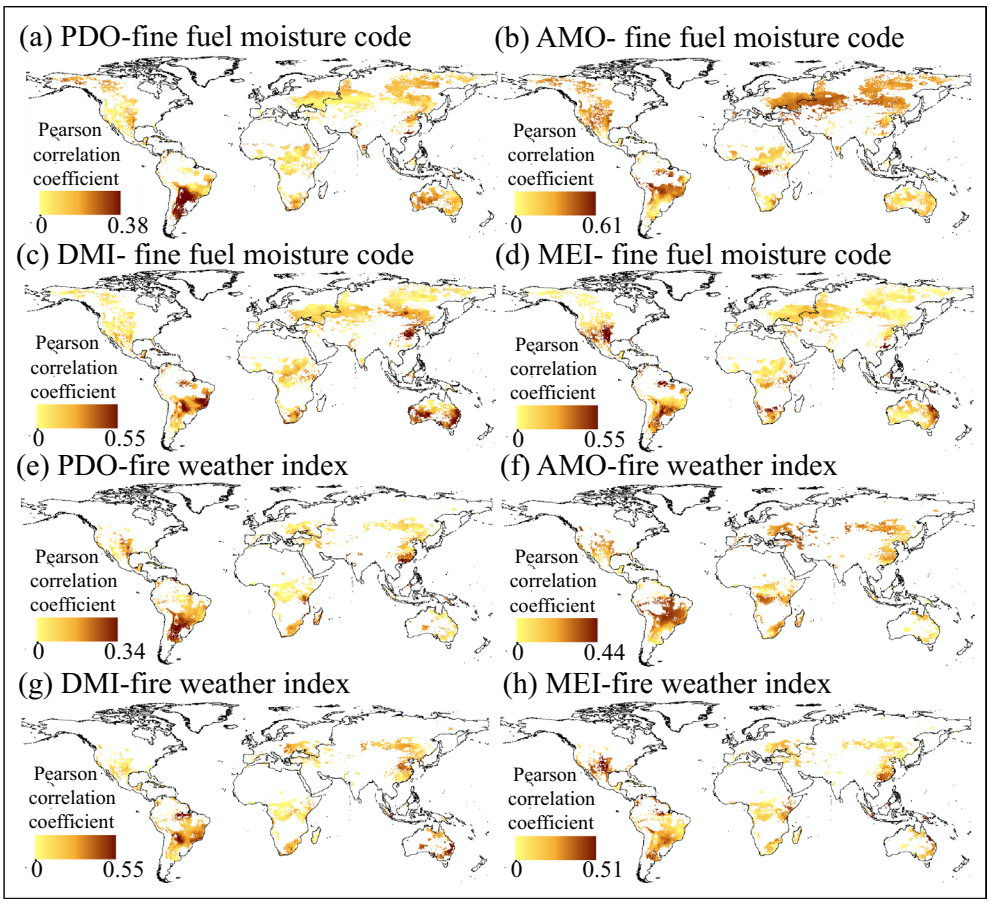

Fig. 10 Distribution map-3 of correlation coefficients of atmospheric–oceanic indices and wildfire-related variables. This dstribution map-3 shows the effects of the four atmospheric-oceanic indices on fine fuelmoisture code and fire weather index through pearson correlation coefficients. Blank indicates thatno wildfires or change-points have occurred on the grid. PDO: Pacific Decadal Oscillation Index.MEI: Multivariate El Niño-Southern Oscillation Index. AMO: Atlantic Multi-decadal OscillationIndex. DMI: Dipole Mode Index

abrupt temperature changes are dominant in temperature-dominated zones. The duff moisture code, fine fuel moisture code, and fire weather index, which have similar change-point distributions, are the main components of duff-, fuel- and fire weather-dominated zones 1 and 2. Different change-point dates distinguish these two clusters. Most of abrupt changes in zone 1 occurred during 1995–2000, while most of abrupt changes in zone 2 occurred during 2000–2005.

Conclusions

This research provides insight into the nonstationarity of wildfire weather during the past four decades by detecting the change-points and long-term trends of six variables connected to wildfires around the world. The results were also discussed within 27 global climate reference regions and an attempt was made to establish a link between change-points of these six variables and atmospheric–oceanic indices. We also did a broad

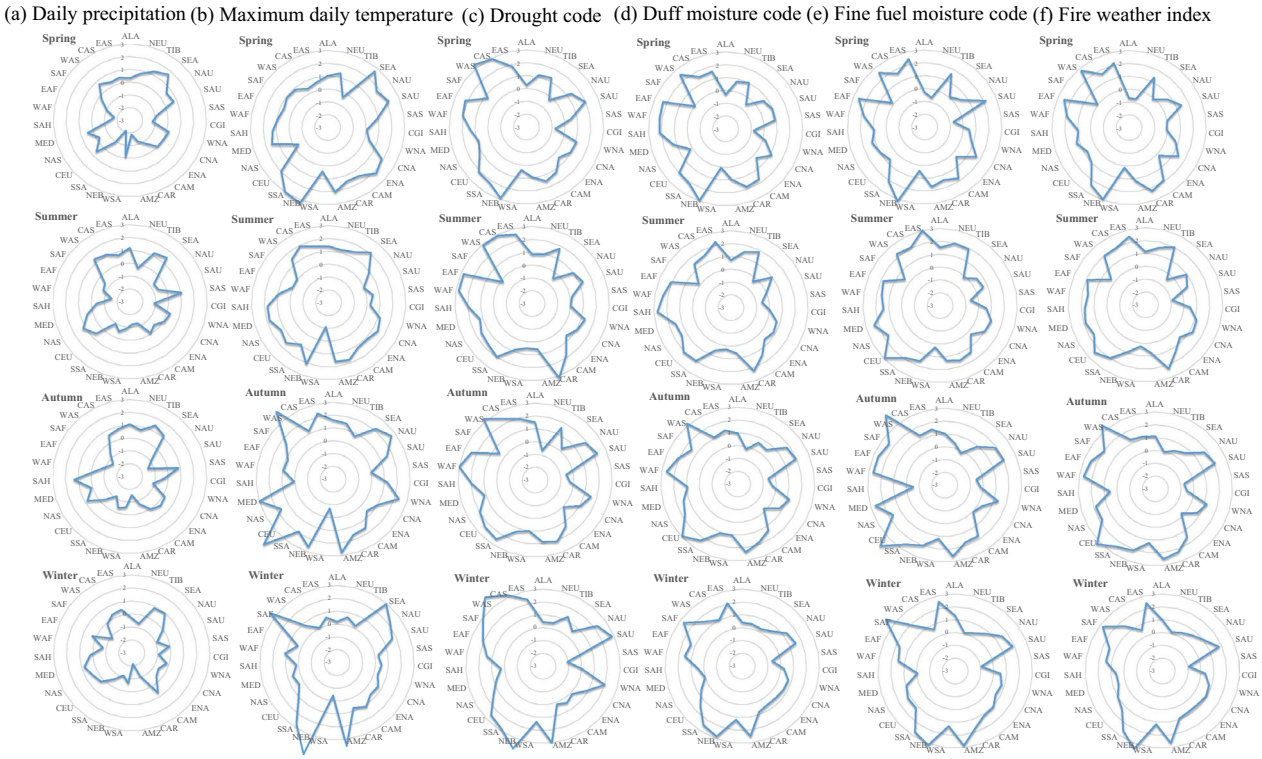

Fig. 11 Different seasonal trends on six continents for the six wildfire-related variables. This figure shows the long-term trends over four seasons for six fire-related variables across 27 climate reference regions. The numbers in the figure are the Z values in the TFPW-MK test. The trend categories according to the Z values are: [1.96, +∞), significant increasing trend; [1.64, 1.96), weak increasing trend; [0, 1.64), no significant increasing trend; (-1.64, 0), no significant decreasing trend; (-1.96, -1.64], weak decreasing trend; (-∞, -1.96], significant decreasing trend

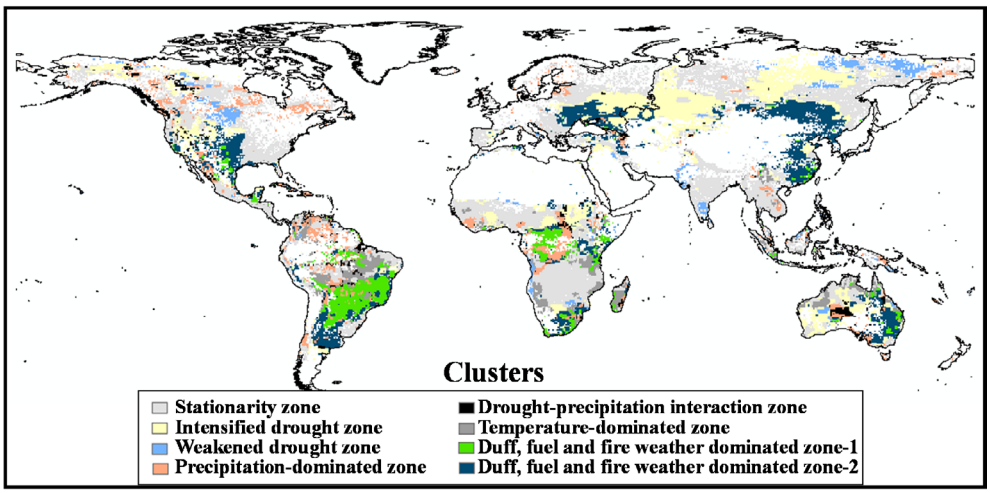

Fig. 12 Cluster map of the change-point dates and change trends among the six wildfire-related variables. This figure shows clustering of change-point dates and change trends, with different coloursindicating different wildfire weather characteristics. For example, the black areas of Australia inthe figure indicate that the wildfire weather in that region is controlled by drought and precipitation

analysis of the various seasonal trends of six different variables associated with wildfires on 27 global climate reference regions. In more detail, we merged the data of the change-points with the information pertaining to the various attributes to obtain a comprehensive global map of abrupt changes in where wildfire weather has been influenced, when it has been influenced, and how it has been influenced by abrupt alterations. These findings have the potential to ultimately help increase our understanding of the impacts of anthropogenic climate change on wildfire weather.

Specifically, the main conclusions of this paper are as follows:

1) The change-point of precipitation, temperature, and drought code mainly occurred in 1995–2000, while the main change-point date of duff moisture code, fine fuel moisture code, and fire weather index was 2000–2005.
2) Correlations between atmospheric–oceanic indices and six wildfire-related variables were discussed, with the most prominent combinations being: AMO-precipitation in the WAF region, MEI + DMI-temperature in AMZ and NEB regions, DMI-drought code in the SAU region, and PDO-duff moisture code + fine fuel moisture code + fire weather index in SSA region.
3) Eight sub-regions with various characteristics, such as a sub-region with a predominance of rainfall, a sub-region with a predominance of temperature, etc., were included in a newly created wildfire weather cluster map.

Acknowledgements
The authors declare no conflicts of interest. All the data are available online for free.

Author contributions
Both authors have made a substantial, direct, and intellectual contribution to the work and approved it for publication. Both authors read and approved the final manuscript.

Funding
This work was conducted by Theme 4 of the Advanced Studies of Climate Change Projection (SENTAN Program) Grant Number JPMXD0722678534 and Grant-in-Aid for Scientific Research (B), 2020–2023 (20H02248, Yoshiya Touge) supported by the Ministry of Education, Culture, Sports, Science and Technology (MEXT), Japan.

Data availability
All data used in this study are available online. The time series of atmospheric–oceanic indices was downloaded from National Oceanic and Atmospheric Administration (https://psl.noaa.gov/). CPC Global Temperature data provided by the NOAA/OAR/ESRL PSL, Boulder, Colorado, USA, from their Web site at (https://psl.noaa.gov/data/gridded/data.cpc.globaltemp.html). CPC Global Unified Precipitation data provided by the NOAA/OAR/ESRL PSL, Boulder, Colorado, USA, from their Web site at (https://psl.noaa.gov/data/gridded/data.cpc.globalprecip.html). Wildfire data were downloaded from ESA Climate Office (https://climate.esa.int/en/projects/fire/data/). The fire danger indices (drought code, fine fuel moisture code, duff moisture code, and fire weather index) were downloaded from the Copernicus Emergency Management Service with user registration at (Vitolo et al. 2020) (https://cds.climate.copernicus.eu/cdsapp#!/dataset/cems-fire-historical?tab=overview).

Declarations

Competing interests
The authors declare that they have no competing interests.

Received: 19 May 2022 Accepted: 1 December 2022
Published online: 05 January 2023

References

Abatzoglou JT, Williams AP (2016) Impact of anthropogenic climate change on wildfire across Western US forests. Proc Natl Acad Sci 113:11770–11775. https://doi.org/10.1073/pnas.1607171113
Addisu S, Selassie YG, Fissha G, Gedif B (2015) Time series trend analysis of temperature and rainfall in lake Tana Sub-basin, Ethiopia. Environ Sys Res 4:1–12. https://doi.org/10.1007/s10668-020-01192-0
Ahmadi F, Nazeri Tahroudi M, Mirabbasi R, Khalili K, Jhajharia D (2018) Spatiotemporal trend and abrupt change analysis of temperature in Iran. Meteorol Appl 25:314–321. https://doi.org/10.1002/met.1694
Asfaw A, Simane B, Hassen A, Bantider A (2018) Variability and time series trend analysis of rainfall and temperature in northcentral Ethiopia: a case study in Woleka sub-basin. Weather Clim Extrem 19:29–41. https://doi.org/10.1016/j.wace.2017.12.002
Ayamga J, Pabi O, Amisigo BA, Fosu-Mensah BY, Codjoe SNA (2021) Annual and intra-annual climate variability and change of the Volta Delta, Ghana. Environ Monit Assess 193:1–19. https://doi.org/10.1007/s10661-021-08986-3
Aziz R, Yucel I, Yozgatligil C (2020) Nonstationarity impacts on frequency analysis of yearly and seasonal extreme temperature in Turkey. Atmos Res 238:104875. https://doi.org/10.1016/j.atmosres.2020.104875
Beaulieu C, Chen J, Sarmiento JL (2012) Change-point analysis as a tool to detect abrupt climate variations. Phil Trans R Soc a: Math Phys Eng Sci 370:1228–1249. https://doi.org/10.1098/rsta.2011.0383
Bedia J, Herrera S, Gutiérrez JM, Benali A, Brands S, Mota B, Moreno JM (2015) Global patterns in the sensitivity of burned area to fire-weather: implications for climate change. Agric Meteorol 214:369–379. https://doi.org/10.1016/j.agrformet.2015.09.002
Bradley PS, Fayyad U, Reina C (1998) Scaling EM (expectation-maximization) clustering to large databases. Microsoft Research:0–25. https://www.microsoft.com/en-us/research/wp-content/uploads/2016/02/tr-98-35.pdf
Byakatonda J, Parida B, Moalafhi D, Kenabatho PK (2018) Analysis of long term drought severity characteristics and trends across semiarid Botswana using two drought indices. Atmos Res 213:492–508. https://doi.org/10.1016/j.atmosres.2018.07.002
Ca VT (2017) A climate change assessment via trend estimation of certain climate parameters with in situ measurement at the coasts and islands of Viet Nam. Climate 5:36. https://doi.org/10.3390/cli5020036
Carney M, Azencott R, Nicol M (2020) Nonstationarity of summer temperature extremes in Texas. Int J Climatol 40:620–640. https://doi.org/10.1002/joc.6212
Carvalho A, Flannigan MD, Logan K, Miranda AI, Borrego C (2008) Fire activity in Portugal and its relationship to weather and the Canadian fire weather index system. Int J Wildland Fire 17:328–338. https://doi.org/10.1071/WF07014
Chen M, Shi W, Xie P, Silva VB, Kousky VE, Wayne Higgins R, Janowiak JE (2008) Assessing objective techniques for gauge-based analyses of global daily precipitation. J Geophys Res: Atmospheres. https://doi.org/10.1029/2007JD009132

Chou C, Chiang JC, Lan C-W, Chung C-H, Liao Y-C, Lee C-J (2013) Increase in the range between wet and dry season precipitation. Nat Geosci 6:263–267. https://doi.org/10.1038/NGEO1744
Chuvieco E, Pettinari M, Lizundia-Loiola J, Storm T, Padilla Parellada M (2018) ESA Fire Climate Change Initiative (Fire_cci): MODIS Fire_cci Burned Area Pixel product, version 5.1. Centre for Environmental Data Analysis [data set]. https://doi.org/10.5285/58f00d8814064b79a0c49662ad3af537.
Damberg L, AghaKouchak A (2014) Global trends and patterns of drought from space. Theoret Appl Climatol 117:441–448. https://doi.org/10.1007/s00704-013-1019-5
Das J, Jha S, Goyal MK (2020) Non-stationary and copula-based approach to assess the drought characteristics encompassing climate indices over the Himalayan states in India. J Hydrol 580:124356. https://doi.org/10.1016/j.jhydrol.2019.124356
Dempster AP, Laird NM, Rubin DB (1977) Maximum likelihood from incomplete data via the EM algorithm. J Roy Stat Soc: Ser B (methodol) 39:1–22. https://doi.org/10.1111/j.2517-6161.1977.tb01600.x
Deng Y, Jiang W, He B, Chen Z, Jia K (2018) Change in intensity and frequency of extreme precipitation and its possible teleconnection with large-scale climate index over the China from 1960 to 2015. J Geophys Res: Atmospheres 123:2068–2081. https://doi.org/10.1002/2017JD027078
Dhakal N, Jain S, Gray A, Dandy M, Stancioff E (2015) Nonstationarity in seasonality of extreme precipitation: a nonparametric circular statistical approach and its application. Water Resour Res 51:4499–4515. https://doi.org/10.1002/2014WR016399
Dong Z, Wang L, Sun Y, Hu T, Limsakul A, Singhruck P, Pimonsree S (2021) Heatwaves in Southeast Asia and their changes in a warmer world. Earth's Future 9:e202EF1001992. https://doi.org/10.1029/2021EF001992
Erdman C, Emerson JW (2008) A fast Bayesian change point analysis for the segmentation of microarray data. Bioinformatics 24:2143–2148. https://doi.org/10.1093/bioinformatics/btn404
Fox D, Carrega P, Ren Y, Caillouet P, Bouillon C, Robert S (2018) How wildfire risk is related to urban planning and Fire Weather Index in SE France (1990–2013). Sci Total Environ 621:120–129. https://doi.org/10.1016/j.scitotenv.2017.11.174
Fraley C, Raftery AE, Murphy TB, Scrucca L (2012) mclust version 4 for R: normal mixture modeling for model-based clustering, classification, and density estimation. Technical Report No. 597. https://stat.uw.edu/sites/default/files/files/reports/2012/tr597.pdf
Fraley C, Raftery AE (2002) Model-based clustering, discriminant analysis, and density estimation. J Am Stat Assoc 97:611–631. https://doi.org/10.1198/016214502760047131
Fryzlewicz P (2014) Wild binary segmentation for multiple change-point detection. Ann Stat 42:2243–2281. https://doi.org/10.1214/14-AOS1245
Ge Y, Apurv T, Cai X (2016) Spatial and temporal patterns of drought in the continental US during the past century. Geophys Res Lett 43:6294–6303. https://doi.org/10.1002/2016GL069660
Geirinhas JL, Russo A, Libonati R, Sousa PM, Miralles DG, Trigo RM (2021) Recent increasing frequency of compound summer drought and heatwaves in Southeast Brazil. Environ Res Lett 16:034036. https://doi.org/10.1088/1748-9326/abe0eb
Glantz MH (2001) Currents of change: impacts of El Niño and La Niña on climate and society. Cambridge University Press, England
Gu X, Zhang Q, Li J, Singh VP, Sun P (2019) Impact of urbanization on nonstationarity of annual and seasonal precipitation extremes in China. J Hydrol 575:638–655. https://doi.org/10.1016/j.jhydrol.2019.05.070
Harris S, Lucas C (2019) Understanding the variability of Australian fire weather between 1973 and 2017. PLoS ONE 14:e0222328. https://doi.org/10.1371/journal.pone.0222328
Haynes K, Fearnhead P, Eckley IA (2017) A computationally efficient nonparametric approach for changepoint detection. Stat Comput 27:1293–1305. https://doi.org/10.1007/s11222-016-9687-5
IPCC (2014) Climate Change 2014: Synthesis Report. Contribution of Working Groups I, II and III to the Fifth Assessment Report of the Intergovernmental Panel on Climate Change. IPCC, Geneva, Switzerland. https://archive.ipcc.ch/pdf/assessment-report/ar5/syr/SYR_AR5_FINAL_full_wcover.pdf
Ivancic TJ, Shaw SB (2017) Identifying spatial clustering in change points of streamflow across the contiguous US between 1945 and 2009. Geophys Res Lett 44:2445–2453. https://doi.org/10.1002/2016GL072444
Jiang S, Wang M, Ren L, Xu CY, Yuan F, Liu Y, Lu Y, Shen H (2019) A framework for quantifying the impacts of climate change and human activities on hydrological drought in a semiarid basin of Northern China. Hydrol Process 33:1075–1088. https://doi.org/10.1002/2016GL072444
Kane R (1999) Rainfall extremes in some selected parts of Central and South America: ENSO and other relationships reexamined. Int J Climatol: J R Meteorol Soc 19:423–455. https://doi.org/10.1002/(SICI)1097-0088(19990330)19:43.0.CO;2-O
Kärner O (2002) On nonstationarity and antipersistency in global temperature series. J Geophys Res. https://doi.org/10.1029/2001JD002024
Kendall, MG (1948) Rank Correlation Methods. Griffin, London.
Kwon H-H, Lall U (2016) A copula-based nonstationary frequency analysis for the 2012–2015 drought in California. Water Resour Res 52:5662–5675. https://doi.org/10.1002/2016wr018959
Larrain H, Ugarte A, Pinto R, Cereceda P, Lázaro P, Osses P, Schemenauer R (2001) Three years of zoological records at a fog-site of Alto Patache, south of Iquique (Chile), during 'El Nino'and 'La Nina'(1997–2001). II Conference on Fog and Fog Collection, Saint John, NF, Canada. pp 297–300. https://www.angelfire.com/ex/niebla/pdf/zoolconf.PDF
Liu Y, Liu B, Yang X, Bai W, Wang J (2015) Relationships between drought disasters and crop production during ENSO episodes across the North China Plain. Reg Environ Change 15:1689–1701. https://doi.org/10.1007/s10113-014-0723-8
Liu S, Kang W, Wang T (2016) Drought variability in Inner Mongolia of northern China during 1960–2013 based on standardized precipitation evapotranspiration index. Environ Earth Sci 75:145. https://doi.org/10.1007/s12665-015-4996-0
Liu M, Liu P, Guo Y, Wang Y, Geng X, Nie Z, Yu Y (2020) Change-point analysis of precipitation and drought extremes in china over the past 50 years. Atmosphere 11:11. https://doi.org/10.3390/atmos11010011
MacQueen J (1967) Some methods for classification and analysis of multivariate observations. Proceedings of the fifth Berkeley symposium on mathematical statistics and probability. Oakland, CA, USA. pp 281–297
Mann HB (1945) Nonparametric tests against trend. Econometrica: J Econometric Soc. https://doi.org/10.2307/1907187
McKay CP, Friedmann EI, Gómez-Silva B, Cáceres-Villanueva L, Andersen DT, Landheim R (2003) Temperature and moisture conditions for life in the extreme arid region of the Atacama Desert: four years of observations including the El Nino of 1997–1998. Astrobiology 3:393–406. https://doi.org/10.1089/153110703769016460
Meshram SG, Singh VP, Meshram C (2017) Long-term trend and variability of precipitation in Chhattisgarh State, India. Theoret Appl Climatol 129:729–744. https://doi.org/10.1007/s00704-016-1804-z
Mueller SE, Thode AE, Margolis EQ, Yocom LL, Young JD, Iniguez JM (2020) Climate relationships with increasing wildfire in the southwestern US from 1984 to 2015. For Ecol Manage 460:117861. https://doi.org/10.1016/j.foreco.2019.117861
Mukherjee S, Mishra A, Trenberth KE (2018) Climate change and drought: a perspective on drought indices. Curr Clim Change Rep 4:145–163. https://doi.org/10.1007/s40641-018-0098-x
O'Dell K, Ford B, Fischer EV, Pierce JR (2019) Contribution of wildland-fire smoke to US PM2. 5 and its influence on recent trends. Environ Sci Technol 53:1797–1804. https://doi.org/10.1021/acs.est.8b05430
Ouhamdouch S, Bahir M (2017) Climate change impact on future rainfall and temperature in semi-arid areas (Essaouira Basin, Morocco). Environ Processes 4:975–990. https://doi.org/10.1007/s40710-017-0265-4
Pan Y, Wang W, Shi W (2019) Assessment of CPC global daily surface air temperature (CPC-T2m) analysis. Assessment, Science and Technology Infusion Climate Bulletin, NOAA's National Weather Service [data set], 22:24. https://downloads.psl.noaa.gov/Datasets/cpc_global_temp/
Panthou G, Mailhot A, Laurence E, Talbot G (2014) Relationship between surface temperature and extreme rainfalls: a multi-time-scale and event-based analysis. J Hydrometeorol 15:1999–2011. https://doi.org/10.1175/JHM-D-14-0020.1
Pettitt AN (1979) A non-parametric approach to the change-point problem. J Roy Stat Soc: Ser C (appl Stat) 28:126–135. https://doi.org/10.2307/2346729
Qu Y, Montzka C, Vereecken H (2021) Causation discovery of weather and vegetation condition on global wildfire using the PCMCI Approach. 2021 IEEE International Geoscience and Remote Sensing Symposium IGARSS. IEEE. pp 8644–8647. https://doi.org/10.1109/IGARSS47720.2021.9553155

Salman SA, Shahid S, Ismail T, Chung E-S, Al-Abadi AM (2017) Long-term trends in daily temperature extremes in Iraq. Atmos Res 198:97–107. https://doi.org/10.1016/j.atmosres.2017.08.011
Sanabria J, Bourrel L, Dewitte B, Frappart F, Rau P, Solis O, Labat D (2018) Rainfall along the coast of Peru during strong El Niño events. Int J Climatol 38:1737–1747. https://doi.org/10.1002/joc.5292
Scott AJ, Knott M (1974) A cluster analysis method for grouping means in the analysis of variance. Biometrics: 507–512. https://doi.org/10.2307/2529204
Scrucca L, Fop M, Murphy TB, Raftery AE (2016) mclust 5: clustering, classification and density estimation using Gaussian finite mixture models. The R Journal 8:289. https://www.ncbi.nlm.nih.gov/pmc/articles/PMC5096736/
Sharples JJ, Lewis SC, Perkins-Kirkpatrick SE (2021) Modulating influence of drought on the synergy between heatwaves and dead fine fuel moisture content of bushfire fuels in the Southeast Australian region. Weather Clim Extrem 31:100300. https://doi.org/10.1016/j.wace.2020.100300
Slater LJ, Anderson B, Buechel M, Dadson S, Han S, Harrigan S, Kelder T, Kowal K, Lees T, Matthews T (2021) Nonstationary weather and water extremes: a review of methods for their detection, attribution, and management. Hydrol Earth Syst Sci 25:3897–3935. https://doi.org/10.5194/hess-25-3897-2021
Takahashi K (2004) The atmospheric circulation associated with extreme rainfall events in Piura, Peru, during the 1997–1998 and 2002 El Niño events. Ann Geophys. https://doi.org/10.5194/angeo-22-3917-2004
Tangang F, Juneng L, Aldrian E (2017) Observed changes in extreme temperature and precipitation over Indonesia. Int J Climatol 37:1979–1997. https://doi.org/10.1002/joc.4829
Tehrany MS, Jones S, Shabani F (2019) Identifying the essential flood conditioning factors for flood prone area mapping using machine learning techniques. CATENA 175:174–192. https://doi.org/10.1016/j.catena.2018.12.011
Tian X, McRae DJ, Jin J, Shu L, Zhao F, Wang M (2011) Wildfires and the Canadian forest fire weather index system for the Daxing'anling region of China. Int J Wildland Fire 20:963–973. https://doi.org/10.1071/WF09120
Trollope W, Trollope L, Hartnett D (2002) Fire behaviour a key factor in the ecology of African grasslands and savannas. Proceedings of IV International Conference on Forest Fire Research & Wildland Fire Safety. pp 18–23. http://talltimbers.org/wp-content/uploads/2014/03/Trollope2007_op.pdf
Vitolo C, Di Giuseppe F, Barnard C, Coughlan R, San-Miguel-Ayanz J, Libertá G, Krzeminski B (2020) ERA5-based global meteorological wildfire danger maps. Scientific Data 7:1–11. https://doi.org/10.1038/s41597-020-0554-z
Vu TM, Mishra AK (2019) Nonstationary frequency analysis of the recent extreme precipitation events in the United States. J Hydrol 575:999–1010. https://doi.org/10.1016/j.jhydrol.2019.05.090
Ward JH Jr (1963) Hierarchical grouping to optimize an objective function. J Am Stat Assoc 58:236–244. https://doi.org/10.2307/2282967
Westerling AL, Hidalgo HG, Cayan DR, Swetnam TW (2006) Warming and earlier spring increase western U.S. forest wildfire activity. Science 313:940–943. https://doi.org/10.1126/science.1128834
Wu P-Y, You GJ-Y, Chan M-H (2020) Drought analysis framework based on copula and Poisson process with nonstationarity. J Hydrol 588:125022. https://doi.org/10.1016/j.jhydrol.2020.125022
Xie P, Chen M, Yang S, Yatagai A, Hayasaka T, Fukushima Y, Liu C (2007) A gauge-based analysis of daily precipitation over East Asia. J Hydrometeorol 8:607–626. https://doi.org/10.1175/JHM583.1
Xie P, Chen M, Shi W (2010) CPC unified gauge-based analysis of global daily precipitation. Preprints, 24th Conf on Hydrology, Atlanta, GA, Amer Meteor Soc,
Ye L, Shi K, Xin Z, Wang C, Zhang C (2019) Compound droughts and heat waves in China. Sustainability 11:3270. https://doi.org/10.3390/su11123270
Yue S, Wang CY (2002) Applicability of prewhitening to eliminate the influence of serial correlation on the Mann-Kendall test. Water Res Res. https://doi.org/10.1029/2001WR000861

Publisher's Note